Tweed, Twins, and Holes

Ekhard K.H. Salje

Department of Earth Sciences, Cambridge University, Downing Street, Cambridge CB2 3EQ, UK

Abstract

Tweed, twin and porous microstructures are traditionally studied in mineralogy to understand the thermal history of minerals, and to identify their properties such as chemical transport and elastic behavior. Recently, the same research area has blossomed in material sciences and physics with the aim to design and build devices which are based on the properties of nano-structures. Only the very existence and the properties of tweed, twins, and holes matters in this quest while the crystalline matrix plays only a minor role in the current search for novel device materials. This development has largely bypassed mineralogists while physicists did not profit from the age-long experience of mineralogists in dealing with such materials.

In this outlook-paper I will first discuss some key findings and approaches to foster the transfer of ideas in both directions: mineralogists can potentially inspire material scientists while the physics of the fine structure of twin walls and tweed can help mineralogists to understand mineral properties in much more detail than hereto possible. Besides the observation that novel

physical properties can spring from microstructures, most recent work also includes the dynamics of microstructures under external stress or electric fields. The dynamics is virtually always non-smooth or ‘jerky’. One of the best studied jerk distribution is that of collapsing porous minerals under stress, where the main focus of research is the identification of precursor effects as warning signs for larger events such as the collapse of mines, boreholes or even regional earth quakes. The underlying physics is the same as in large earth quakes (which can always be modeled but not observed in laboratory experiments). The agreement between laboratory experiments of porous collapse and large scale earth quakes goes well beyond the quake statistics and includes waiting time distributions and the Omori law of after-shocks. The same approach is used to characterize high-tech materials in aircraft industry and functional materials.

Introduction

Functional properties at a nano-scale, their statics and dynamics, was investigated in major research initiatives for over 30 years in several disciplines. The relevant nano-structures are, in order of increasing intrusiveness to the matrix: tweed, (transformation-) twins and holes which have been used to develop device materials for industrial applications while they naturally exist in many minerals. Tweed and twins in ferroelastic minerals develop when structural phase transitions occur with a loss of point group symmetry elements results in transformation twinning in the low temperature phase (Salje 2012). Tweed represents a 'precursor' for twin boundaries in the low symmetry phase (Bratkovsky et al. 1994 a-c, Khachaturian 1983, Parlinski et al 1993 a,b, Castan et al. 1999). Holes in porous structures often stem from phase mixtures when one phase has been eliminated or where this phase was a gas as in case of volcanic ejecta.

The existence of microstructures with functional properties has opened a new research field in physics and materials science in which the functionality of a device material is no longer expected to be present in the bulk of the material but located in its nanoscopically small regions such as twin boundaries. This approach is summarized as 'domain boundary engineering' in the physics literature (Salje 2010, Salje and Zhang 2009). Nanostructures have always been a major research topic in mineralogy simply because they are common in minerals (Fig 1) and it may be possible to reconstruct the thermal history of a mineral by exploring their heterogeneities (e.g. Tullis 1980, David et al. 1995, Vernon and Paterson 2008, Trepman and Stokhert 2001, Vernon 1999, Zhang et al. 1996, Palmer et al. 1989, Salje and Wruck 1983). However, it has not inspired mineralogists to extend their data to find 'unusual' twin boundaries with functionalities such as conductivity, transport, polarity and magnetism. Synthetic porous structure are shown in Fig.3 and contain similar functionalities near their extremely extended surfaces. Such materials are

omnipresent as high-tech materials from cooking pans to aircraft stabilizers. Besides the current focus on this research in physics and materials sciences we find that much of the fundamental descriptive work was done already in mineralogy, often published in American Mineralogist over more than 5 decades.

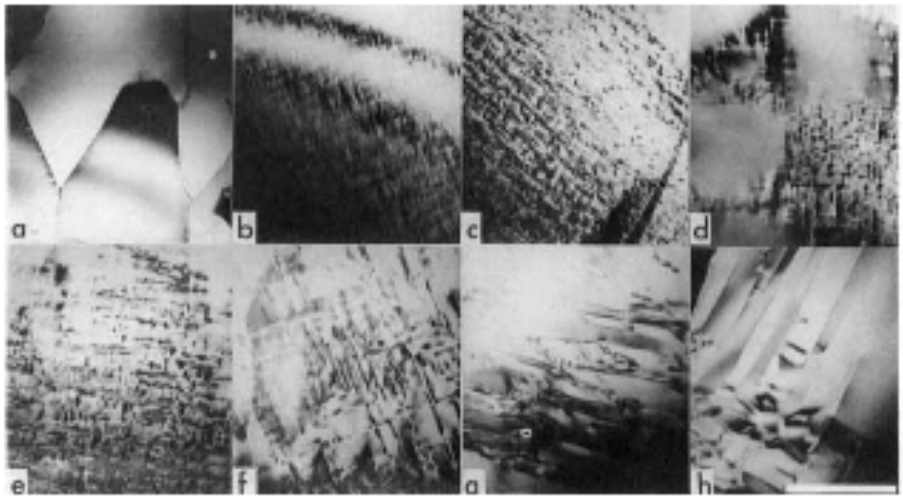

Fig. 1 Transmission electron micrographs illustrating the typical evolution of microstructures observed during the transformation from hexagonal to orthorhombic cordierite. At 1673 K the transformation sequence is from (a) to (b), the finer scale of nucleation or orthorhombic cordierite appearing to produce a continuously coarsening microstructure. The length of the scale bar is 0. 2 μm. (after Putnis and Salje, 1994). Twins are seen in (a) and (h) while tweed is typical for (b). The other images show mixtures between the two domain structures.

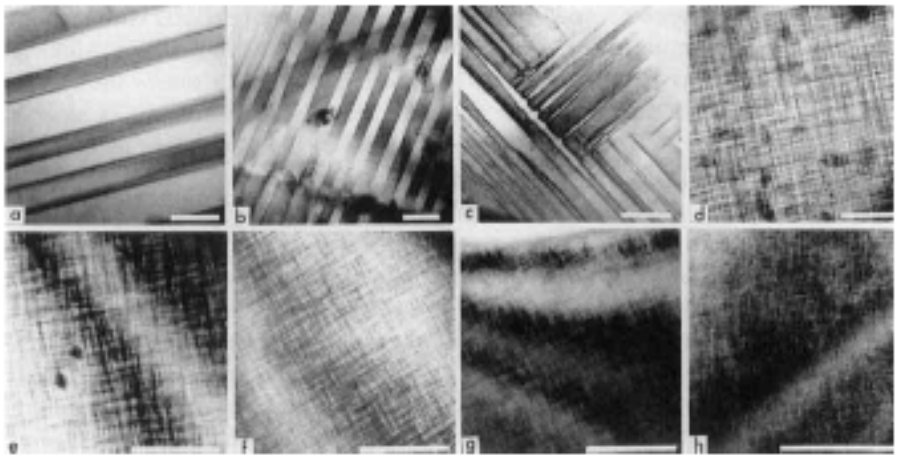

Fig. 2 Electron micrographs of {ll0}-type twin modulations in $YBa_2(Cu,Co)_3O_{7-\delta}$ with the incident beam parallel to [001]. Length of scale bar : 0.l μm. The twin structure transforms from a coarse twin (a) to a stripe pattern (b) and a junction pattern (c) to various forms of tweed (after Schmahl et al., 1989).

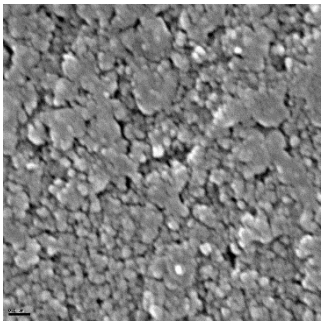

Fig.3 porous structures in a synthetic SiO_2 glass, vycor (after Aufort at al. 2014)

Tweed and twin structures

Tweed forms when local fluctuations become large and lead to atomic displacements which form interwoven pattern of local strain. The orientation of the strain pattern is usually related to the soft elastic directions of a material. Early structural investigations of martensitic phase transformations revealed a pretransitory phenomena that was sandwiched between the high temperature austenite and low temperature martensite phase regions, over a narrow temperature range near the transition temperature (Tullis 1980, Tsatskis and Salje 1996, Kartha et al. 1995). Tweed is characterized by a crosshatching in the bright-field images, are oriented along particular crystallographic directions, and are up to a hundred angstroms in length. Upon approaching the transition temperature on cooling, the tweed structures became increasingly pronounced and eventually evolved into the long-range ordered low temperature martensitic polydomain structure. Bratkovsky et al. (1994 a-c) have simulated the ordering of tweed structures into thin microdomains and the subsequent coarsening of the thin microdomains into a more traditional domain structure. Themodynamic fluctuations were shown to control the length and width of the tweeds. Texturing and coarsening were controlled by long range elastic strains, which resulted in an ordering of the embryos. These simulations revealed a common sequence of domain states that could be achieved by varying degrees of elastic ordering, temperature, and defects. Kartha et al. (1995) have considered the effect of quenched disorder on the evolution of tweed structures towards the twinned phase. More recently, the topic of long-time metastable tweed precursor states have been reinvestigated and referred to as domain glasses (Salje et al. 2014) and other glass states (Wang et al. 2006).

Another approach to produce tweed is to increase of twin densities. Increasing the twin boundary density is possible by cold stressing a sample (Ding et al. 2012, Salje et al. 2012). In minerals,

this can happen by rock mechanics where geological processes lead to stress induced changes of microstructures. This method was shown to be more effective for the nucleation of fine scale, complex twin patterns than thermal quench. Twin densities very close to the structural limit where the spacers between the twin boundaries with a boundary width of w reach 10 w can be achieved. With w = 1 nm one would expect a lower limit for the bulk spacer of some >10 nm. Experimentally distances of 100 nm have been commonly observed. The reason for the limit of the boundary density implies the competition between tweed and twin structures (Shapiro et al. 1991). This phenomenon is probably widespread in minerals such as alkali-feldspar (e.g. Tsatskis and Salje 1996) and orthoclase (Fig. 4).

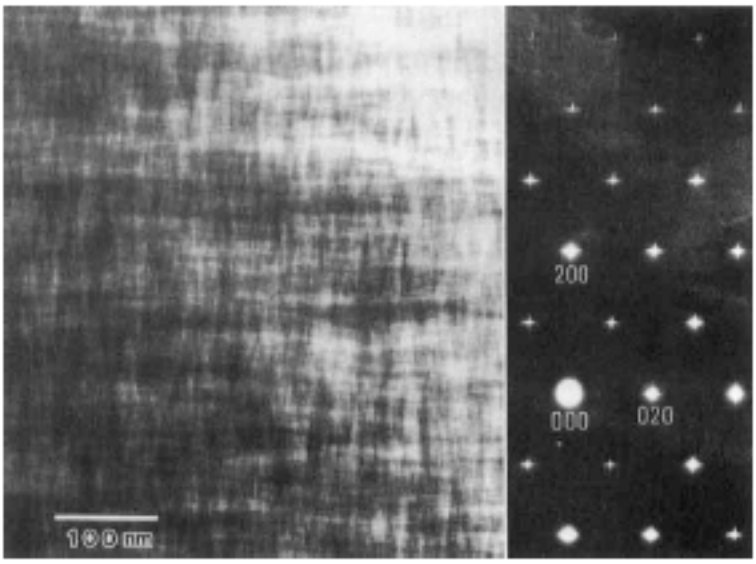

Fig. 4 Bright field transmission electron micrograph (and its associated electron diffraction pattern) showing the tweed microstructure observed in K-feldspar (after McLaren and Fitzgerald 1987).

Fig. 5 Three dimensional representation of diffuse scattering profile associated with a tweed microstructure in a superconducting oxide sample in Fig. 2 (reanalyzed after Locherer et al. 1996).

The diffraction pattern of tweed is shown in the insert of Fig.4 and in Fig.5. It is characterized by a 4-armed starfish (or clover) patterns. Each of the branches in Fig. 5 extends along a direction perpendicular to the modulation wavefront. The intensity profile does not show any maxima as expected for incommensurate structures but decays monotonically from the zone center over some 0.1 reciprocal lattice units. This diffraction signal can refer either to static tweed (structural modulation, chemical exsolution etc.) or dynamic tweed where the pattern fluctuates with time. The latter case of dynamic tweed is often referred to as 'flicker tweed' to indicate that the deformation waves are not pinned but move through the sample. Flicker tweed would not be seen in transmission electron microscopy while diffraction measures the autocorrelation (the Patterson function) of the modulation and detects dynamic tweed.

Functionality

Tweed and twin pattern can host properties which do not exist in the bulk. Typical examples are electrical or ionic conductivity, polarity and magnetism. The probably most notable local

property is superconductivity in an isolating perovskite, namely WO_3 and its derivatives (Aird and Salje 1998, 2000, Kim et al. 2010, Salje et al. 1978) (Fig. 6). Another example is the formation of dipolar layers in $CaTiO_3$ (Van Aert et al. 2012, Goncalves-Ferreira et al. 2008, 2010) (Fig.7) $SrTiO_3$ and $BaTiO_3$ (Zykova-Timan and Salje 2014, Salje et al. 2013 a,b,d , Scott et al. 2012, Blinc et al 2005, Kampe et al. 2014).

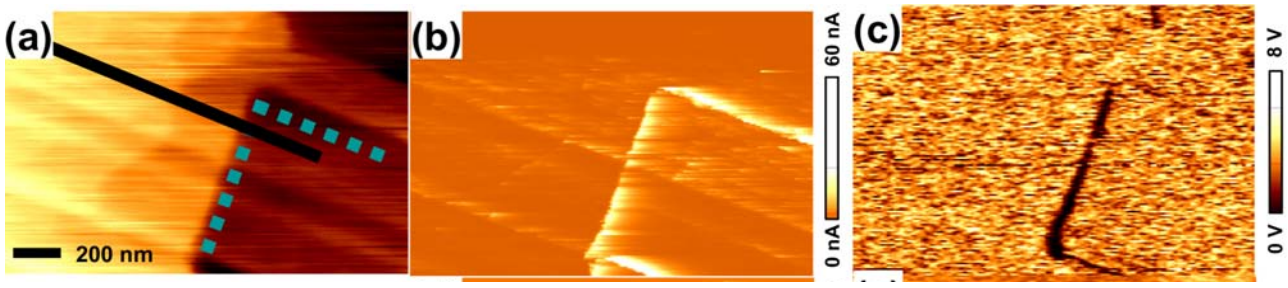

Fig. 6 Superconducting twin boundaries in WO_3 (after Kim et al. 2010) with the tological, curent and piezoelectric contrast across the same twin boundary.

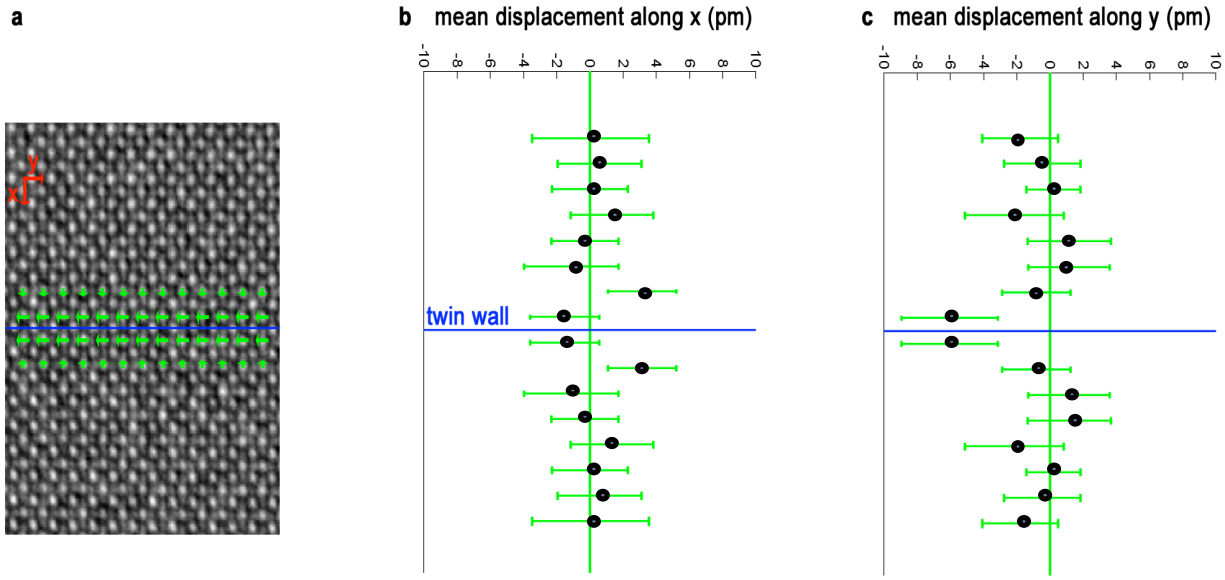

Fig.7 Polar twin boundaries in $CaTiO_3$. Displacements of Ti atoms near the twin boundary (a). The blue horizontal line shows the position of the twin wall. b) Mean interatomic Ti–Ti column distances perpendicular to the twin wall, averaged in the direction parallel with the twin wall, together with their 90% confidence intervals. c) Mean interatomic Ti–Ti column distances parallel to the twin wall, averaged in the direction parallel with the twin wall, together with their 90% confidence intervals (after Van Aert et al. 2012). The overall mirror plane symmetry of the twin wall is preserved (Yokota et al. 2014))

Twin boundaries and tweed represent nanostructures are predestined to interact with other order parameters (e.g. Lottermoser et al.2009). In perovskites this situation is particularly simple: the structural order parameter may be the octahedra tilt Q. This octahedral tilt reduces the off-centering of the atom in the octahedra midpoint. The coupling between the two parameters is hence repulsive. In a Landau potential the coupling term is formulated as $\lambda Q^n P^m$ where the faintness indices n and m are determined by symmetry. The most common coupling scheme (which is always allowed by symmetry) is $n = m = 2$. This coupling is called bi-quadratic and has been analyzed in much detail by Houchmandzadeh et al. (1991) and Conti et al. (2011). Repulsive coupling means $\lambda > 0$ and interfacial functionality means that $P = 0$ in the bulk. With the Landau functional written as

$$L_\lambda(Q,P) = (1 - Q^2)^2 + (1 - P^2)^2 + \lambda Q^2 P^2 - c_\lambda \quad (2)$$

$$G_{\kappa,\lambda}[Q,P] = \int L_\lambda(Q,P) + |Q'|^2 + \kappa |P'|^2 \, dx \quad (3)$$

where the dash means the first spatial derivative of Q or P, respectively. The full phase diagram of this potential in Fig. 8 was derived by Conti et al. (2011). Here we concentrate on the conditions $P = 0$ in the bulk. This condition is met inside the interval $\lambda > 2$ below the bend curve

expanding to larger values of λ. This condition means that the repulsive force needs to be large enough to destroy P in the bulk but not in the twin boundary and that the intrinsic wall thicknesses κ limits the value of λ to $\lambda < 2 + 4/\kappa$. In these cases the twin boundary in Q will always host a local parameter P which represents the functionality of the wall.

Other coupling schemes were explored by Salje and Carpenter (2011) and gradient coupling (Zhao et al. 2015) will not be considered in this report. In tweed structures, a similar coupling scheme applies and has been described by Salje and Aktas (2014).

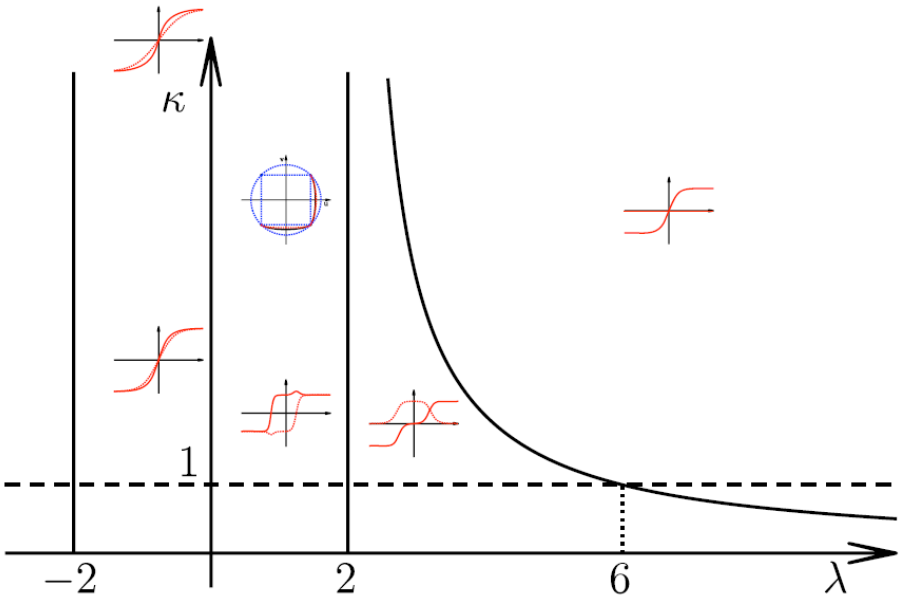

Fig. 8 Phase diagram of in the *(λ, κ)* plane. Only the region $\lambda > -2, \kappa > 0$ gives rise to interfaces between stable phases (after Conti et al. 2011).

Collapse: the hole story

The dynamics of functional tweed and twin boundaries are surprisingly un-smooth (Salje and Dahmen, 2014). When external forces are applied to change the domain pattern, the pattern often

reacts by jerky movements, only in case of very mobile pattern in adaptive structures (Viehland and Salje, 2014) are such 'jerks' or spikes are replaced by continuous movements. The origin of jerks is sometimes related to pinning of microstructures to impurities - while Peierls pinning is rather uncommon (Goncalves-Ferreira 2010, Lee et al. 2006). Impurity pinning is not the only or even the most common reason, however, because microstructures also jam. Jamming means that the movement of part of the pattern is hindered by other parts of the pattern. No defects or impurities are needed for this mechanism (Salje et al. 2011). Jamming produces 'crackling noise' namely a sequence of jerks which follow an extremely well defined statistical pattern which is very close to the Gutember-Richter law in earth quakes (Setna et al. 2001, Salje and Dahmen 2014, Baro et al. 2013). The concept of jerks and crackling noise has hence been around for a long time, but hardly ever applied to minerals. Starting with Barkhausen analysis of magnetization jumps in slowly magnetized ferromagnets, it was generalized to 'crackling noise' because it was found that similar phenomena are much more wide spread than just in magnetism (Setna et al.2001). Other fields that show crackling noise include: granular materials (Salje 2012, Jaeger et a. 1996, Dahmen et al. 2011) collapse of porous materials (Salje et al. 2011, 2013, Baró et al. 2013, Ben-Zion et al. 2011) plasticity in small crystals (Zaiser 2006,Dahmen et al. 2009.), change in the co-existence interval of stepwise structural phase transitions (Salje 2012, Romero et al. 2011), transitions in Mott insulators (Lashley et al. 2014), decision making processes (Friedman et al. 2012) etc. Materials applications were initially in martensitic alloys, and in magnetic materials (for nondestructive materials testing), geophysical applications in earth quakes etc.

Many systems with crackling noise show similar statistics. For example it has been shown experimentally and theoretically that the size distribution of magnetization avalanches of soft

magnetic materials, observed as Barkhausen noise, decays with the same power law as the slip-size distribution of slowly compressed samples (Zaiser 2006; Dahmen et al. 2009; Galam 1997. Miguel and Zapperi 2006, Tsekenis et al. 2013, Dimiduk et al.. 2006; Friedman et al. 2012; Harrison and Salje 2010, 2011; Csikor et al. 2007,). Renormalization group calculations suggest that on long length scales the systems flow to the same fixed point under coarse graining, which suggests that their scaling behavior on long length scales is the same (Richeton et al. 2005, Sethna et al. 2001). In fact, all systems described by the well known "interface depinning universality class" flow to the same fixed point as these two systems (Zaiser 2006, Richeton et al. 2005). Big open questions concern the size of the underlying universality class, i.e. how many systems show the same crackling noise statistics.

For mineralogists the outstanding system where such universal jerks properties can be measured with great accuracy is the collapse of porous minerals. They can serve as a model system for a wide variety of systems ranging from earth quakes to ferroelectric device materials and poling of magnetic minerals in paleomagnetism. Porous minerals are important in their own right too: they are widely used in filtering, separation, medical transplants and others (Kim et al. 2012; Petri et al. 2008; Gallardo et al. 2010; Salje, Koppensteiner et al. 2009). Understanding porous materials remains one of the great challenges in mining, building industry and geology. Mining is often done in environments containing porous mineral assemblies (Salje et al. 2013; Manosa et al. . 2000), including goethite, pyrite and coal, which may lead to serious accidents when landslides occur in open mining or when mining shafts collapse. Such catastrophic events are sometimes announced by acoustic precursors of the collapse (Zhao et al. 2013; Salje et al. 2013, Castillo-Villa et al. 2013). The typical failure under shear stress is that porous material 'snaps'

when exposed to the critical shear stress. Crack propagation is fast and few intermediate states were observed at low temperatures. Snapping becomes more viscous for torsion pendulum experiments at high temperatures near the melting point where grain boundary sliding and dislocation creep become dominant (e.g. Gibson and Ashby 1999). In a recent study, Salje et al. 2011) used a porous SiO_2 glass material (Vycor) to show that these avalanches follow almost perfect power law statistics ('crackling noise') with a characteristic critical exponents similar to those measured in mechanical instabilities in martensites and ferroelastic materials, critical dynamics in micro fracturing (Kashef et al. 2011) and spontaneous AE in volcanic rocks. This has put the problem of understanding the failure of porous materials under compression within the scenario of crackling noise and avalanche criticality.

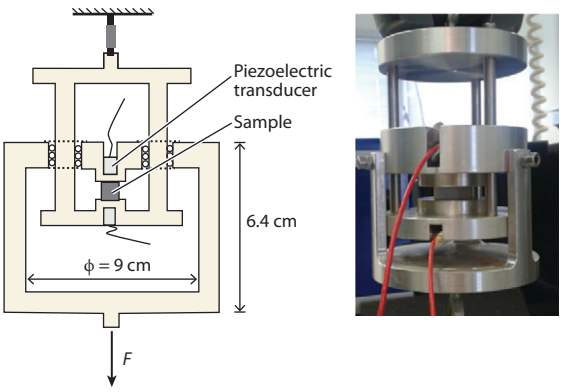

Fig.9 Experimental arrangement for measurements of the collapse under applied stress in porous materials. The collapse is measured by the relative length change of the sample and by the acoustic emission (AE) of jerks during the compression. The squared time derivative of the length change $(dX/dt)^2 \propto v^2$ is proportional to the acoustic activity (counts per second) so that both data sets are used for the determination of the jerk statistics. The AE measures the energy emission of the sample, which often follows a power-law distribution with exponent ε.

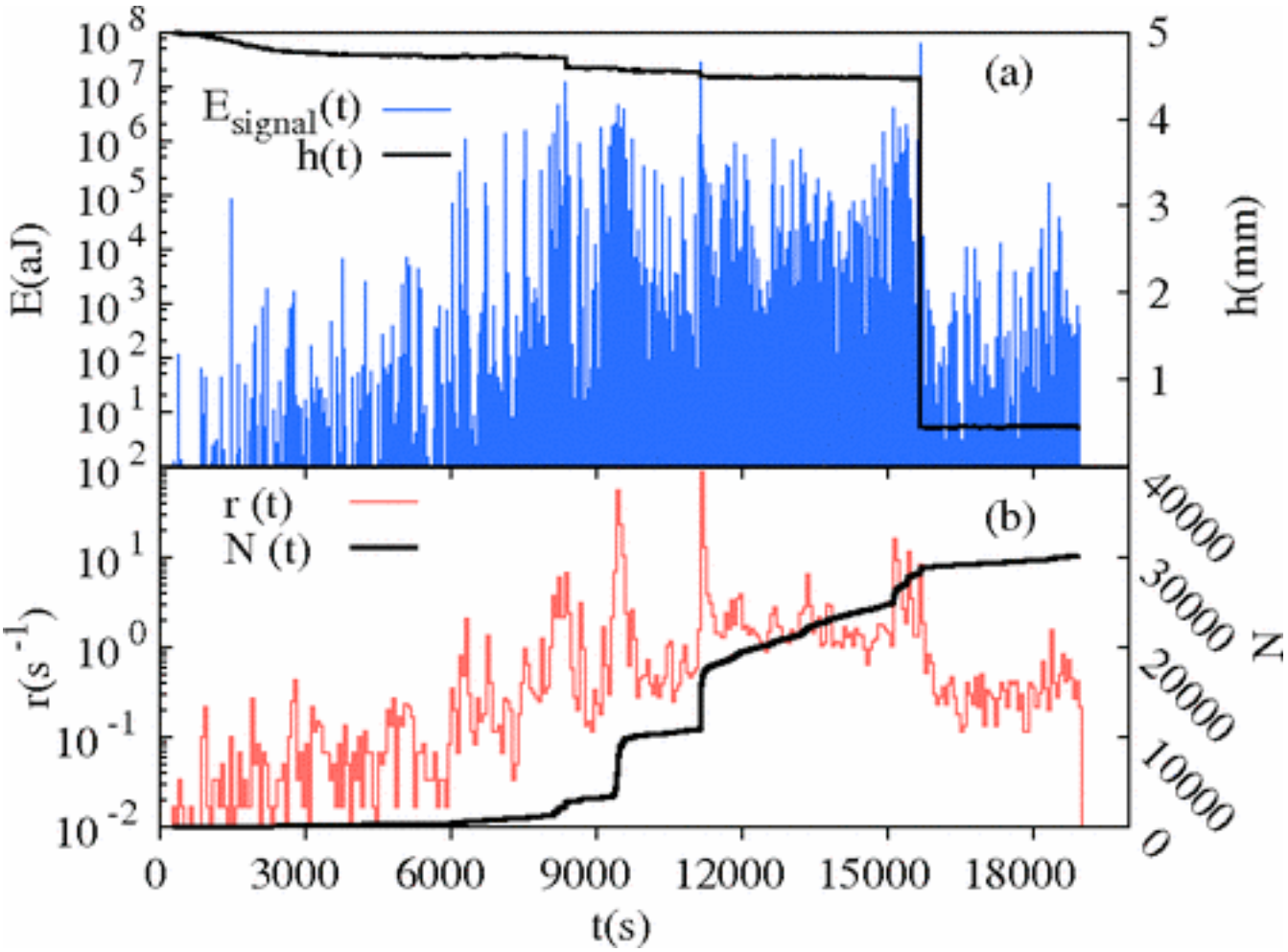

Fig.10 Typical compression jerk spectra as obtained by Baró et al. (2013). (a) The outcome of compression on the specimen height (h) as a function of time (t) (time is proportional to stress, as the experiment was undertaken under a constant stress rate) and the energy of the acoustic emission (AE) avalanches, shown on a logarithmic scale. (b) Time evolution of the AE activity rate and of the total number of events. Abbreviations: E_{signal}, acoustic emission signal; h(t), changing height of the sample; N(t), accumulated rate; r(t), rate of the acoustic emission signal.

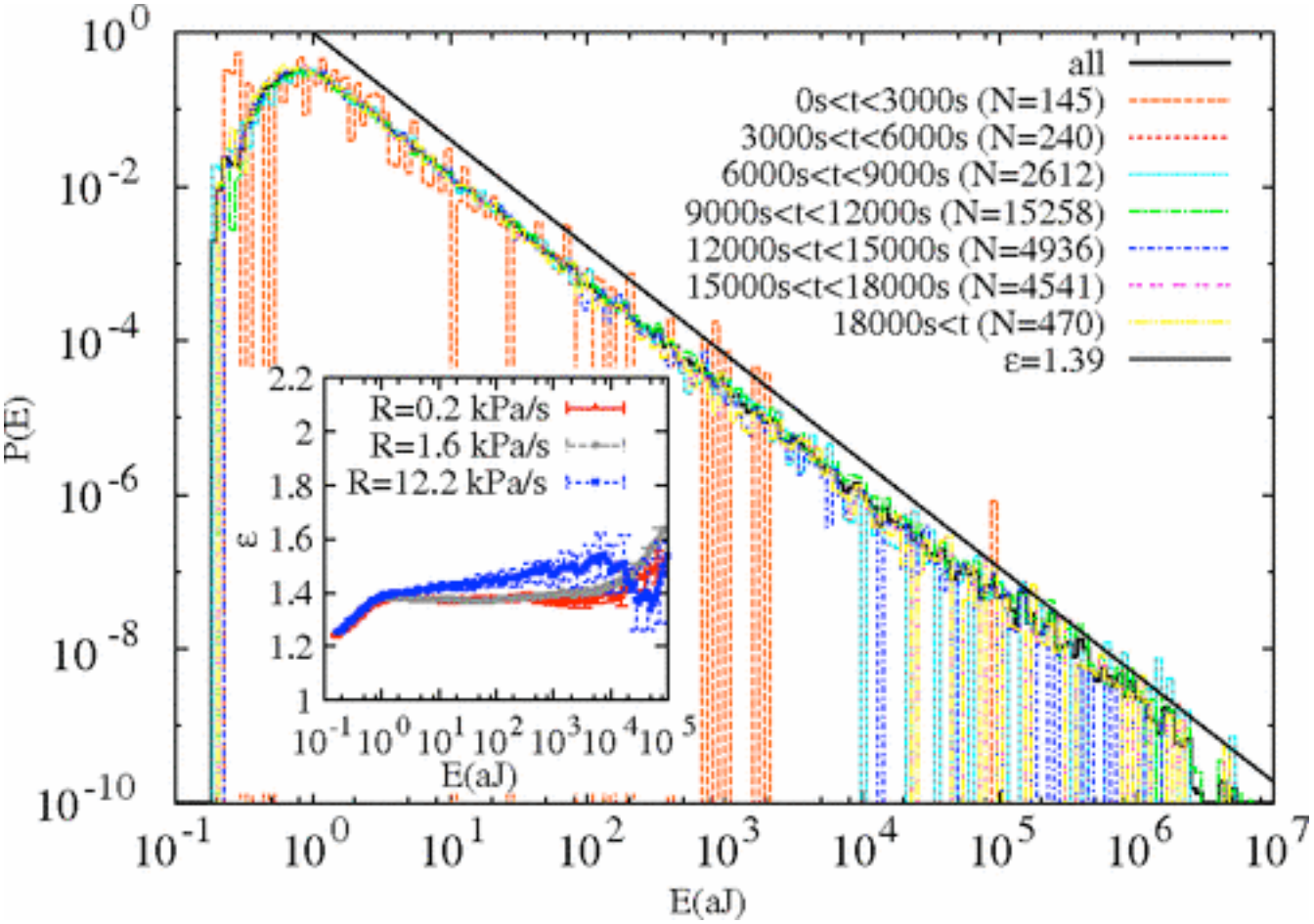

Fig.11 Distribution of avalanche energies during the full experiment with 7 different subperiods. The line shows the behavior corresponding to ε = -1.39. The inset shows the ML-fitted exponent as a function of a lower threshold E_{min} for the three experiments.

The acoustic activity is not restricted to the time intervals of the collapse but is not restricted to the time interval of the collapse but occurs over the whole time span of the experiment. Even at times after the collapse, the debris contains still porous but intact regions which collapse when

the stress is increased further. In the log-log plot in Figure 11 the energy distribution p(E) of jerks is shown as function of the energy E. As can be seen the histograms are quite linear in this plot. This suggests again that the distribution energies is a power law: of

$$P(E)\, dE \sim E^{-e} / E^{1-e}$$

where E_{min} is a lower cutoff used for normalization. The lines in Figure 11 are guides to the eye. They already reveal the increasing value of the exponent ε with porosity. Interestingly the Vycor sample with a porosity of 40% shows features similar to those of the least porous goethite samples: a similar noise spectrum with no detectable noise gap after the major collapse. The major difference between goethite and Vycor is that the Vycor sample shows a power law distribution of the acoustic emission spectra over a very large interval of six orders of magnitude. In contrast, the power law approximation is found to hold in goethite only for three orders of magnitude while deviations occur for higher energy events. Furthermore the power-law exponents for goethite are larger than the value of 1.39 of the Vycor sample. Otherwise, it appears that the noise detection, and hence the analysis of potential early warning noise before collapses is independent of the composition of the material and depends only on its porosity. Baro et al. (2013) investigated SiO_2 based materials including sandstone and synthetic glasses and found that the noise statistics is very similar for all of them. The close connection to the earth quake statistics, including waiting times and after-shock probablilities have lead to the notion that earth quakes (or their proxys) can be investigated experimentally (and not jut by simulation) in the laboratory (Biswas et al. 2013; Main et al. 1989).

Resonant piezoelectric spectroscopy

Polar behavior (ferroelectric/piezoelectric/ferrielectric behavior) in tweed, twin walls, and near surfaces in porous minerals relates to a very small number of atoms which constitute a tiny percentage of the sample (typically 0.1 ppm). This means that their piezoelectric signal is quite weak and a very sensitive experimental technique is needed for this investigation. One of the best tools for the detection of weak polarity is second harmonic generation microscopy (SHG). Second-harmonic generation has been reviewed as a tool for studying polarity, electronic and magnetic structures of crystals in Fiebig et al. (2005). However, one has to be careful with the interpretation of SHG data because local defects can easily induce SHG signal (Bleser et al. 1994, Meier et al. 2010, Becker and Bohatý 2010, Lottermoser et al. 2009; Frey and Payne 1996; Yokota et al. 2014)

A new experimental technique, resonant piezoelectric spectroscopy (RPS) has been introduced (Salje et al. 2013, Aktas et al. 2013, Aktas et al. 2013). The experimental arrangement for resonant piezoelectric spectroscopy (RPS) is shown in Fig. 11. If the sample is piezoelectric, the AC voltage applied between two parallel surfaces of the sample leads to the oscillation of domain boundaries. This oscillation creates strain fields proportional to the electric field and forms elastic waves propagating in the sample. If the frequency of the elastic wave corresponds to one of the natural frequencies of the sample, it becomes resonant and its amplitude increases drastically. This mechanical resonance condition makes RPS highly sensitive to polar ordering even at nano scales. The detection of resonant elastic standing waves, (i.e. mechanical resonances), is then achieved using a piezoelectric detector attached at one end of an alumina rod which transmits any signal received from the sample to the piezoelectric detector. Note the

similarity between the experimental arrangements of RPS and RUS (Salje et al. 2013). In RUS, elastic waves are generated mechanically by the application of an AC voltage across a piezoelectric transducer (top transducer in Fig. 12). In RPS the AC voltage is applied across the sample, which would generate elastic waves only if the sample, locally or macroscopically, shows piezoelectric behavior.

As an example, RPS measurements were performed on quartz, which were performed with an AC voltage of 20 V applied across two parallel surfaces in the basal plane of the sample. Segments of spectra collected between 300 K and 1050 K are shown in Fig. 13. The spectrum shown in green is assumed to be collected at the α-β transition at T_c = 846 K, where α corresponds to the low temperature phase with the point group 32 while β is the high temperature phase that belongs to the point group 622. There are mechanical resonances peaks

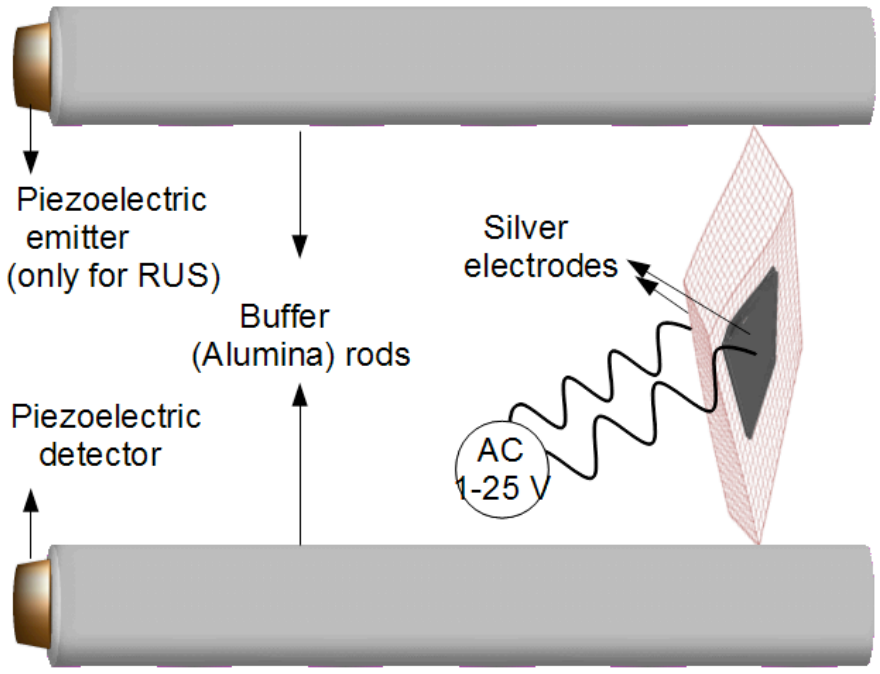

Figure 12: Schematic diagram of the experimental arrangement for resonant piezoelectric spectroscopy (RPS). The same setup can be used for resonant ultrasonic spectroscopy (RUS) by applying the AC voltage across the top piezoelectric transducer rather than the electrodes coating two parallel surfaces of the sample. An AC voltage of 1-25 V is applied across the sample.

both below and above T_c, which indicates piezoelectricity in both phases. This is consistent with the symmetry properties of the α and β phases. In the α phase the piezoelectric coefficients d_{11} and d_{14} are active, while in the β phase only d_{14} is active (Ohno et al. 2006). Monotonous temperature behavior of resonance amplitudes at T_c implies that resonances are excited mainly by the piezoelectric coefficient d_{14}. Elastic properties of quartz have been determined in great detail elsewhere (Carpenter, Salje, Graeme-Barber 1998) and will not be discussed in this review. However, it is worth noting that in the spectra shown in Fig. 13 those resonances where the frequencies do not change significantly with temperature belong to alumina rods. Other resonances, which show a frequency dip at T_c , belong to the quartz

sample. The square of a resonant frequency is proportional to the effective elastic constant associated with the resonance. Therefore, the observed softening in resonant frequencies is in agreement with earlier reports of the co-elastic nature of quartz.

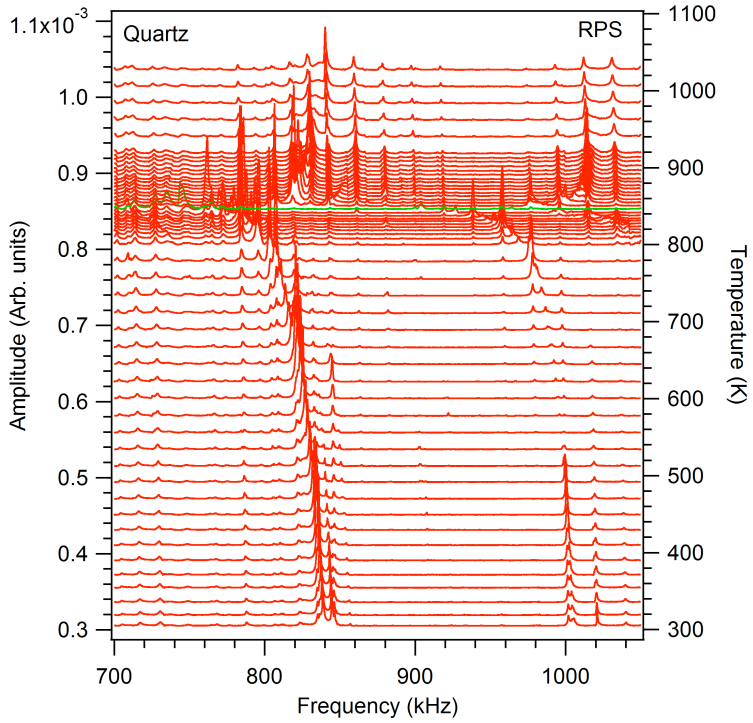

Figure 13: RPS spectra of quartz collected between 300 K and 1040 K. The spectrum shown in green is assumed to be collected at T_c = 846 K. Left axis represents the amplitude. The spectra were translated vertically in proportion to the temperatures at which they were collected as to label the right axis as temperature.

The same experimental method was now employed to observed polar domain walls. RPS spectra of paraelectric $SrTiO_3$ were collected between 15 K and 100 K and are shown in Fig. 14. Upon cooling, peaks associated with mechanical resonances of the $SrTiO_3$ sample appear below 80 K, which is well below the ferroelastic transition temperature T_c = 105 K. As the temperature is reduced, the amplitudes of resonance peaks reach their maximum values below 40 K.

Considering that bulk $SrTiO_3$ shows no ferroelectric or piezoelectric behavior, the observed piezoelectric behavior indicates that twin walls become polar below 80 K.The gradual increase in amplitudes implies that piezoelectricity inside twin walls increases upon cooling and leads to the mobility of twin walls and hence proves the functionality of twin walls in $SrTiO_3$. RPS is hence shown to be sensitive enough to observe these microstructure-related polarities even when the number of atoms in the polar state is very small. It is a method, which may be able to find such states in minerals where polarity was not reported before.

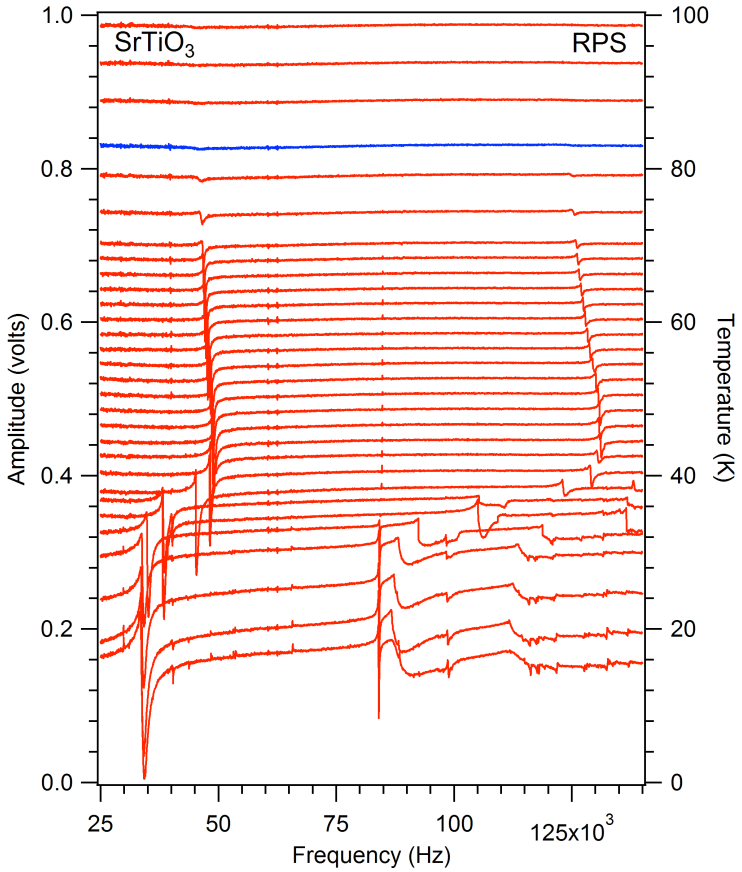

Fig. 14: Low temperature RPS spectra of $SrTiO_3$. Panel (a) Segments of RPS spectra in the frequency interval from 25 kHz to 100 kHz. The left axis represents the amplitude and the right axis gives the temperature at which each spectrum was collected. The spectrum shown in

blue was collected at T^* ~ 80 K, below which $SrTiO_3$ shows piezoelectricity that originates from ferroelastic twin walls. The spectrum shown in green was collected at the cubic-tetragonal ferroelastic transition temperature T_c = 105 K.

The polarity in twin boundaries of SrTiO3 was confirmed by computer simulations (Zykova-Timan and Salje, 2014) where the local structure is not simply an array of dipoles in the wall but contains vortices which lead to rotations of ferroelectric dipoles as shown in Fig.15. It was shown subsequently that the direction of these dipoles can be switched by electric fields, which demonstrates that twin boundaries in perovskite structures are indeed functional in several chemical compounds. We expect that more examples will be found in future with some of these examples coming from mineralogical collections.

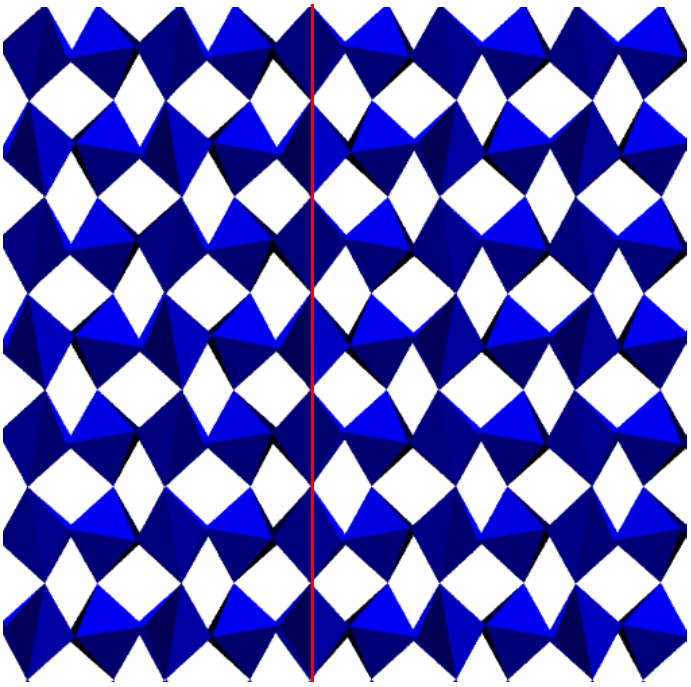

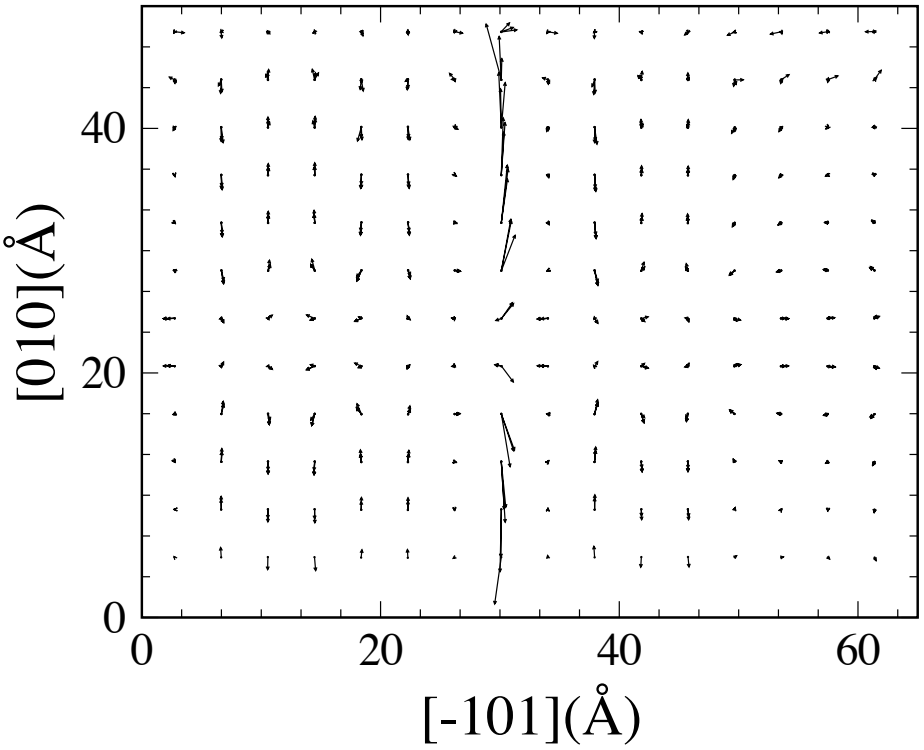

Fig. 15. Twin boundary in SrTiO3 with the octahedral rotation disappearing in the wall (top) and the corresponding displacements of Ti away from the center of the oxygen octahedral. These displacements constitute dipoles, which can be switched by electric fields. These twin boundaries are functional ferroelectrics.

The implications of our results are wide-ranging. First, we cannot take it for grated anymore that ionic transport id dominated by the transport coefficients of the bulk material. Whenever the interfacial density is high, then we can short-cut the bulk and transport mainly through the network of interfaces. This effect is even greater when electronic transport (or hole transport) is considered. A few superconducting interfaces will always electrically shorten the bulk so

that the properties of the bulk become irrelevant compared with the interfaces. We have given a general scheme to quantify the coupling between the order parameter and other quantities such as polarity and conductivity. While these results will probably not falsify any previous results, they add another dimension. Minerals may be high-tech materials, we simply do not know. We are in a similar situation as in the beginning of research on ferroelectric materials in the 1950s: many of the first surveys were then conducted in mineralogical collections where minerals were systematically tested for their ferroelectric behavior. Later, the same happened for magnetic materials. Today we should test domain boundary properties and also their dynamic behavior. There is a lot to do!

Acknowledgements:

The authors is grateful to the Leverhulme foundation (RG66640) and EPSRC (RG66344) for financial support.

References:

Aird, A. and Salje E.K.H. (2000) Enhanced reactivity of domain walls in with sodium, European Journal of Physics B, 15, 205–210.

Aird, A. and Salje, E.K.H. (1998) Sheet superconductivity in twin walls: experimental evidence, J. Phys.: Condens. Matter, 10, L377.

Aktas, O., Carpenter, M.A. and Salje, E.K.H. (2013) Polar precursor ordering in BaTiO3 detected by resonant piezoelectric spectroscopy, Applied Physics Letters, 103, 142902.

Aktas, O., Salje, E. K. H., Crossley, S., Lampronti, G. I., Whatmore, R. W., Mathur, N. D. and Carpenter, M. A. (2013) Ferroelectric precursor behavior in PbSc0.5Ta0.5O3 detected by field-induced resonant piezoelectric spectroscopy, Phys. Rev. B 88, 174112.

Aufort, J., Aktas, O. and Salje, E.K.H. (2014) Resonant piezoelectric spectroscopy in SiO2-based materials, in preparation.

Baró, J., Corral, A., Illa, X., Planes, A., Salje, E.K.H., Schranz, W., Soto-Parra, D.E., and Vives, E. (2013) Statistical Similarity between the Compression of a porous material and earthquakes. Physical Review Letters, 110, 088702.

Becker P., and Bohatý L. (2010) Second harmonic generation on incommensurate structures: The case of multiferroic $MnWO_4$, Phys. Rev. B, 82, 155112.

Ben-Zion, Y., Dahmen, K.A and Uhl, J.T. (2011) A Unifying Phase Diagram for the Dynamics of Sheared Solids and Granular Materials, Pure Appl. Geophys. 168, 2221–37.

Biswas, S., Ray, P. and Chakrabarti, B. K. (2013) Equivalence of the train model of earthquake and boundary driven Edwards-Wilkinson interface, Europ. Phys. J. B 86, 388.

Bleser, T ., Berge, B ., Bismayer, U. and Salje, E.K.H. (1994) The possibility that the optical second-harmonic generation in lead phosphate, Pb3(PO4)2 , is related to structural imperfections, J. Phys.: Condens. Matter, 6, 2093-9.

Blinc, R., Zalar, B., Laguta, V.V. and Itoh,M. (2005) Order-disorder component in the phase transition mechanism of ^{18}O enriched strontium titanate. Phys. Rev. Lett., 94,147601.

Bratkovsky, A.M., Marais, S.C., Heine, V., and Salje, E. K. H. (1994) The theory of fluctuations and texture embryos in structural phase transitions mediated by strain. J. Phys.: Condens. Matter, 6, 3679-3696.

Bratkovsky, A. M., Salje, E. K. H., and Heine, (1994) V. Overview of the origin of tweed texture, Phase Transitions, 52, 77–83.

Bratkovsky,A.M., Salje, E. K. H., Marais, S. C., and Heine, V. (1994) Theory and computer simulation of tweed texture. Phase Transitions, 48, 1–13.

Castan, T., Vives, E,, Lindgard, P.A. (1999) Modeling premartensitic effects in Ni2MnGa: A mean-field and Monte Carlo simulation study, Phys. Rev. B 60, 7071-7084.

Castillo-Villa, P. O., Baro, J., Planes, A., Salje, E. K. H., Sellappan, P., Kriven, W. M. and Vives, E. (2013) Crackling noise during failure of alumina under compression: the effect of porosity, Phys. Cond. Matter 25, 292202.

Carpenter, M.A., Salje, E.K.H., Graeme-Barber, A., Wruck, B., Dove, M.T. and Knight, K.S. (1998) Calibration of excess thermodynamic properties and elastic constant variations associated with the alpha <–>beta phase transition in quartz, American Mineralogist, 83, 2–22.

Conti,S., Müller,S., Poliakovsky,A. and Salje,E.K.H. (2011) Coupling of order parameters, chirality, and interfacial structures in multiferroic materials, J. Phys.: Condens. Matter, 23,142203.

Csikor, F.F., Motz, C., Weygand, D., Zaiser, M. and Zapperi, S. (2007) Dislocation avalanches, strain bursts, and the problem of plastic forming at the micrometer scale, Science 318, 251–54.

Dahmen, K.A., Ben-Zion, Y. and Uhl, J.T. (2011) A simple analytic theory for the statistics of avalanches in sheared granular materials, Nat. Phys. 7:554–57.

Dahmen, K.A., Ben-Zion, Y. and Uhl, J.T. (2009) Micromechanical Model for Deformation in Solids with Universal Predictions for Stress-Strain Curves and Slip Avalanches, Phys. Rev. Lett. 102, 175501.

David, F., Walker, F.D.L., Lee, M.R. and Parsons I.(1995) Micropores and micropermeable texture in alkali feldspars, Mineralogical Magazine 59, 505–534 .

Dimiduk, D.M., Woodward, C., LeSar, R. and Uchic, M.D. (2006) Scale-free intermittent flow in crystal plasticity, Science 312, 1188–90.

Ding,X., Zhao, Z., Lookman, T. , Saxena, A. and Salje, E. K. H. (2012) High junction and twin boundary densities in driven dynamical systems, Adv. Mater., 24, 5385–5389.

Fiebig, M., Pavlov, V.V. and Pisarev, R.V. (2005) Second-harmonic generation as a tool for studying electronic and magnetic structures of crystals: review, J. Opt. Soc. Am. B, 22, 96–118.

Frey, M. H. and Payne, D. A. (1996) Grain-size effect on structure and phase transformations for barium titanate, Phys. Rev. B, 54, 3158–3168.

Friedman, N., Ito, S., Brinkman, B.A.W., Shimono, M., DeVille, R.L., Dahmen, K. A., Beggs, J. M. and Butler, T. C. (2012a) Universal Critical Dynamics in High Resolution Neuronal Avalanche Data, Phys. Rev. Lett. 108, 208102.

Friedman, N., Jennings, A.T., Tsekenis, G., Kim, J.Y., Uhl, J.T., Greer, J. R. and Dahmen, K. A. (2012b) Statistics of Dislocation Slip Avalanches in Nanosized Single Crystals Show Tuned Critical Behavior Predicted by a Simple Mean Field Model, Phys. Rev. Lett. 109, 095507.

Galam, S. (1997) Rational group decision making: A random field Ising model at T=O. Phys. A 238, 66–80.

Gallardo, M.C., Manchado, J., Romero, F.J., Del Cerro, J., Salje, E.K.H., Planes, A., Vives, E., Romero, R. and Stipcich, M. (2010) Avalanche criticality in the martensitic transition of Cu67.64Zn16.71Al15.65 shape-memory alloy: A calorimetric and acoustic emission study, Phys. Rev. B 81, 174102.

Gibson, L.J. and Ashby, M.F.(1999) Cellular Solids. Cambridge: Cambridge Univ. Press, Cambridge, UK.

Goncalves-Ferreira, L., Redfern, S.A.T.,Artacho, E. and Salje, E.K.H.(2008) Ferrielectric twin walls in $CaTiO_3$, Phys. Rev. Lett., 101, 097602.

Goncalves-Ferreira, L., Redfern, S.A.T., Artacho, E., Salje, E.K.H. and Lee, W.T. (2010) Trapping of oxygen vacancies in the twin walls of perovskite, Phys. Rev. B, 81, 024109.

Harrison, R.J. and Salje, E.K.H. (2010) The noise of the needle: Avalanches of a single progressing needle domain in LaAlO3, Appl. Phys. Lett. 97, 021907.

Harrison, R.J. and Salje, E.K.H. (2011) Ferroic switching, avalanches, and the Larkin length: Needle domains in LaAlO3, Appl. Phys. Lett. 99, 151915.

Houchmandzadeh,B.,Lajzerowicz,J. and Salje,E. (1991) Order parameter coupling and chirality of domain walls. J. Phys.: Condens. Matter, 3, 5163-5168.

Jaeger, H., Nagel, S.R. and Behringer, R.P. (1996) Granular solids, liquids, and gases, Rev. Mod. Phys. 66, 1259–73.

Kampfe,T., Reichenbach, P. , Schroder, M. , Haußmann, A., Eng , L. M. , Woike, T. and Soergel, E. (2014) Optical three-dimensional profiling of charged domain walls in ferroelectrics by Cherenkov second-harmonic generation Phys. Rev. B 89, 035314.

Kashef, S.,Asgari, A., Hilditch, T.B., Yan, W.Y. ,Goel, V.K. and Hodgson, P.D.(2011) Fatigue crack growth behavior of titanium foams for medical applications, Mater.Sci.Eng.A528, 1602–7.

Kartha,S., Krumhansl, J.A., Sethna, J.P. and Wickham, L.K. (1995) Disorder-driven pretransitional tweed pattern in martensitic transformations, Phys. Rev. B 52, 803-822.

Kartha S.,Castan,T., Krumhansl, J.A., and Sethna,J.P. (1991) Spin-glass nature of tweed precursors in martensittic transformations, Phys. Rev. Lett. 67, 3630-3633.

Khachaturian, A. G.(1983) Theory of Structural Transformations in Solids. Dover Books on Engineering Series. Dover Publications, Incorporated, USA.

Kim, Y., Alexe, M. and Salje, E. K. H. (2010) Nanoscale properties of thin twin walls and surface layers in piezoelectric WO3-x Applied Physis Letters 96, 032904.

Kim JY, Gu X, Wraith M, Uhl JT, Dahmen KA, Greer JR. Suppression of Catastrophic Failure in Metallic Glass-Polyisoprene Nanolaminate Containing Nanopillars (2012) Adv. Funct. Mater. 22, 1972–80.

Lashley, J. C.,Gofryk, K.,Mihaila, B.,Smith, J. L. and Salje, E. K. H. (2014) Thermal avalanches near a Mott transition J.Phys. Condensed Matter 26, 035701.

Lee, W. T.,Salje, E. K. H.,Goncalves-Ferreira, L.,Daraktchiev, M. and Bismayer, U. (2006) Intrinsic activation energy for twin-wall motion in the ferroelastic perovskite CaTiO3 Phys. Rev. B 73, 214110.

Locherer, K.R., Chrosch, J. and Salje, E.K.H. (1998) Diffuse x-ray scattering in WO3, Phase Transitions 67, 51-63.

Lottermoser Th., Meier D., Pisarev R. V. and Fiebig M. (2009) Giant coupling of second-harmonic generation to a multiferroic polarization, Phys. Rev. B, 80, 100101.

Main I.G., Meredith P.G. and Jones C. (1989) A reinterpretation of the precursory seismic B-value anomaly from fracture-mechanics, Geophysical Journal 96, 131-138.

Manosa L., Carrillo L., Vives E., Obrado E., Gonzalez-Comas A. and Planes A. (2000) Acoustic emission at the premartensitic and martensitic transitions of Ni2MnGa shape memory alloy, Mater. Sci. Forum 327-3, 481–84.

McLaren A.C. and Fitz Gerald J.D. (1987) Cbed and alchemi investigation of local symmetry and al, si ordering in k-feldspars. Physics and Chemistry of Minerals, 14, 281–292.

Miguel M.C. and Zapperi S. (2006) Fluctuations in plasticity at the microscale, Science 312, 1151–52.

Meier, D. , Leo, N. , Yuan, G. , Lottermoser, Th., Fiebig, M. , Becker, P. and Bohatý, L. (2010) Second harmonic generation on incommensurate structures: The case of multiferroic $mnwo_4$. Phys. Rev. B, 82, 155112.

Ohno I., Harada K. and Yoshitomi C. (2006) Temperature variation of elastic constants of quartz across the alpha-beta transition, Physics and Chemistry of Minerals 33,1–9.

Parlinski,K., Heine, V., and Salje, E.K.H. (1993 a) Origin of tweed texture in the simulation of a cuprate superconductor, J. Phys.: Condens. Matter, 5, 497-519.

Parlinski, K., Salje, E.K.H., and Heine, V. (1993 b)Annealing of tweed microstructure in high Tc superconductors studied by a computer simulation, Acta Metallurgica et Materialia, 41, 839 – 847.

Palmer D.C., Salje E.K.H. and Schmahl W.W. (1989) Phase Transitions in Leucite – X-ray diffraction studies,Phys. Chem. Minerals 16, 714-719.

Petri A., Baldassarri A., Dalton F., Pontuale G., Pietronero L. and Zapperi S. (2008) Stochastic dynamics of a sheared granular medium, Eur. Phys. J. B 64, 531–35.

Putnis, A. and Salje, E. (1994) Tweed microstructures: Experimental observations and some theoretical models. Phase Transitions, 48, 85–105.

Richeton T., Weiss J., Louchet F. (2005) Breakdown of avalanche critical behaviour in polycrystalline plasticity, Nat. Mater. 4, 465–69.

Romero F.J.,Manchado J., Martin-Olalla J.M.,Gallardo M.C. and Salje E.K.H. (2011) Dynamic heat flux experiments in Cu67.64Zn16.71Al15.65: Separating the time scales of fast and ultra-slow kinetic processes in martensitic transformations, Appl.Phys.Lett. 99, 011906.

Salje E. K. H.,Carpenter M. A.,Nataf G. F.,Picht G.,Webber K., Weerasinghe J.,Lisenkov S. andBellaiche, L. (2013) Elastic excitations in BaTiO3 single crystals and ceramics: Mobile

domain boundaries and polar nanoregions observed by resonant ultrasonic spectroscopy, Phys. Rev. B 87, 014106.

Salje E.K.H. and Aktas O. (2014) Functional twin boundaries and tweed microstructures: a comparison between minerals and device materials, Min Mag , in press,

Salje, E. K. H., Ding, X. , Zhao, Z. , Lookman, T. and Saxena, A. (2011) Thermally activated avalanches: Jamming and the progression of needle domains, Phys. Rev. B, 83, 104109.

Salje E.K.H., Koppensteiner J., Reinecker M., Schranz W. and Planes A. (2009) Jerky elasticity: Avalanches and the martensitic transition in Cu74.08Al23.13Be2.79 shape-memory alloy, Appl. Phys. Lett. 97, 021907.

Salje, E. K. H., Aktas, O., Carpenter, M. A. and Scott J.F. (2013) Domains within Domains and Walls within Walls: Evidence for Polar Domains in Cryogenic SrTiO3, Phys. Rev. Letters 111, 247603.

Salje E.K.H., Lampronti G.I., Soto-Parra D.E., Baró J., Planes A. and Vives E. (2013) Noise of collapsing minerals: Predictability of the compressional failure in goethite mines, Am. Mineral. 98, 609–615.

Salje EKH. (2012) Ferroelastic Materials, Annu. Rev. Mater. Res. 42, 265–83.

Salje, E.K.H., Ding, X. and Aktas, O. (2014) Domain Glass, Phys. Status Solidi B 1–6, DOI 10.1002/pssb.201350242.

Salje, E. K. H., Ding, X. , Zhao, Z. and Lookman T. (2012) How to generate high twin densities in nano-ferroics: Thermal quench and low temperature shear, Appl. Phys. Lett., 100, 222905.

Salje E. K. H. and Carpenter, M. A. (2011) Linear-quadratic order parameter coupling and multiferroic phase transitions, J. Phys.: Condens. Matter, 23, 462202.

Salje E. K. H., Aktas, O., Carpenter, M. A. and Scott J.F. (2013) Domains within Domains and Walls within Walls: Evidence for Polar Domains in Cryogenic SrTiO3, Phys. Rev. Letters 111, 247603.

Salje E., Gehlig R. and Viswanathan K. (1978) Structual phase-transitions in mkixed crystals WxMo1-xO3, J. Solid State Chemistry 25, 239-250.

Salje E. and Wruck B. (1983) Specific heat measurements and critical exponents of the ferroelastic phase-transition in Pb3(PO4)2 and Pb3 (P—xAsxO4)2 , Phys. Rev. B 28, 6510-6518.

Salje, E.K.H. and Dahmen, K.A. (2014) Crackling Noise in Disordered Materials, Annual Review of Condensed Matter Physics 5, 233-254.

Salje, E.K.H. (2010) Multiferroic domain boundaries as active memory devices: Trajectories towards domain boundary engineering. ChemPhysChem, 11, 940–950.

Salje E.K.H., Soto-Parra D.E., Planes A., Vives E., Reinecker M. and Schranz W. (2011) Failure mechanism in porous materials under compression: crackling noise in mesoporous SiO2, Philos. Mag. Lett. 91, 554–60.

Salje E., and Zhang, H. (2009) Domain boundary engineering. Phase Transitions, 82, 452–469.

Schmahl, W. W., Putnis, A., Salje, E. , Freeman, P. , Graeme-Barber, A. , Jones, R., Singh, K. K., Blunt, J. , Edwards, P. P., Loram, J. and Mirza, K. (1989) Twin formation and structural modulations in orthorhombic and tetragonal YBa2(Cu1-xCox)3o7- δ, Philos. Mag. Lett., 60, 241–248.

Scott, J. F., Salje, E. K. H. and Carpenter, M. A. (2012) Domain Wall Damping and Elastic Softening in SrTiO3: Evidence for Polar Twin Walls, Phys. Rev. Lett. 109, 187601.

Sethna, J.P., Dahmen, K.A., Myers, C.R. (2001) Crackling noise. Nature 410, 242-250.

Shapiro,S.M., Yang, B. X., Noda, Y. , Tanner, L. E. and Schryvers D. (1991) Neutron-scattering and electron-microscopy studies of the premartensitic phenomena in Ni_xAl_100-x alloys, Phys. Rev. B, 44, 9301–9313.

Trepmann, C. and Stokhert, B.(2001) Mechanical twinning of jadeite – an indication of synseismic loading beneath the brittle–plastic transition, Int. J Earth Sci., 90, 4–13.

Tsatskis, I. and Salje, E.K.H. (1996) Time evolution of pericline twin domains in alkali feldspars: A computer-simulation study, American Mineralogist 81, 800-810.

Tsekenis G., Uhl J.T., Goldenfeld N. and Dahmen K.A.(2013) Determination of the universality class of crystal plasticity , Europhys. Lett. 101, 36003.

Tullis, T.E. (1980) The use of mechanical twinning in minerals as a measure of shear stress magnitudes, J. Geophys. Res., 85, 6263–6268.

Van Aert,S., Turner,S., Delville,R., Schryvers,D., Van Tendeloo,G. and Salje, E.K.H. (2012) Direct observation of ferrielectricity at ferroelastic domain boundaries in catio3 by electron microscopy. Adv. Mater., 24, 523–527.

Vernon, R.H. and Paterson, S.R. (2008) How late are k-feldspar megacrysts in granites?, Lithos, 104, 327 – 336.

Vernon, R. H. (1999) Quartz and feldspar microstructures in metamorphic rocks, Can. Mineral., 37, 513–524.

Viehland D.D. and Salje E.K.H. (2014) Emergent phenomena in domain boundary dominated materials: adaptive structures and functional twin boundaries Submitted to Adv. Mat.

Wang,Y., Ren,X., and Otsuka, K. (2006) Shape memory effect and superelasticity in a strain glass alloy, Phys. Rev. Lett. 97, 225703.

Yokota H., Usami H., Haumont R., Hicher P., Kaneshiro J., Salje E. K. H. and Uesu Y. (2014) Direct evidence of polar nature of ferroelastic twin boundaries in CaTiO3 obtained by second harmonic generation microscope, Phys. Rev. B 89, 144109

Zaiser M.(2006) Scale invariance in plastic flow of crystalline solids, Adv. Phys. 55, 185–245.

Zhang M.,Wruck B.,Barber A.G.,Salje, E.K.H. and Carpenter, M.A. (1996) Phonon spectra of alkali feldspars: Phase transitions and solid solutions , American Mineralogist 81, 92-104.

Zhao Z., Ding X. and Salje E.K.H. (2015) Why most ferroelastic twin boundaries could be polar, submitted to Phys. Rev. Letters.

Zhao Z, Ding X, Lookman T, Sun J, Salje EKH. Mechanical Loss in Multiferroic Materials at High Frequencies: Friction and the Evolution of Ferroelastic Microstructures (2013) Adv. Mater. 25, 3244–3248.

Zykova-Timan, T. and Salje, E. K. H. (2014) Highly mobile vortex structures inside polar twin boundaries in SrTiO3 , Appl. Phys. Lett. 104, 082907.